Available online at www.sciencedirect.com
ScienceDirect
Journal of Sound and Vibration 305 (2007) 641–658
JOURNAL OF SOUND AND VIBRATION
www.elsevier.com/locate/jsvi

# Input power to waveguides calculated by a finite element method

C.-M. Nilsson, S. Finnveden*

*MWL, Aeronautical and Vehicle Engineering, KTH, SE-100 44 Stockholm, Sweden*

Received 31 August 2006; received in revised form 5 April 2007; accepted 16 April 2007
Available online 20 June 2007

**Abstract**

This paper considers the power injected into waveguide structures from forces that are concentrated along the waveguide but are otherwise arbitrary. The motion of the structure is described by a set of coupled, linear, one-dimensional wave equations. These equations are, in this work, devised by the waveguide finite element method, which is a versatile tool for describing wave motion in general structures that have uniform properties along one direction. Two separate procedures are derived. The first is based on spatial and frequency averaging of a modal solution. The second procedure is based on a spatial Fourier transform, which by nature assumes the waveguide to be infinite. It is shown that, in the limit of zero damping, the two methods are identical. Subsequently input power to a stiffener in a railway car structure is calculated and compared with an in situ measurement, showing a fair agreement.


## 1. Introduction

For the assessment of the severity of a structure's vibration, it is useful to know not only the magnitude of the excitation forces but also the vibrational power they inject into the structure. This is particularly so for high-frequency vibrations of structures described by statistical energy analysis (SEA), since the input power is a critical input datum to such an analysis [1–3]. Moreover, it is an experience shared by many practitioners that if the criteria for the application of SEA are roughly met, see e.g., Ref. [4], and if the magnitude of input power is correct, even a crude SEA model will perform reasonably well. This is so as vibrational energy is a conserved quantity, in contrast to, e.g., vibration velocity or sound pressure.

The literature describes the evaluation of input power to common structural elements such as beams, plates and cylindrical shells and these formulations are made available in commercial SEA codes. For general structures, however, the evaluation must often rely on measurements or detailed numerical analysis, which might prove difficult and costly.

A standard procedure for the evaluation of input power is described in detail for a point-excited plate in "Structure Borne Sound" [1, Chapter IV.4]. Thus, for a random location of the force and small damping, the frequency averaged input power is simply given by a numerical factor, the squared force magnitude, the plate mass and the modal density (number of modes per unit frequency). For structures that have dimensions that

*Corresponding author.
*E-mail address:* svantef@kth.se (S. Finnveden).

0022-460X/$ - see front matter 
doi:10.1016/j.jsv.2007.04.025

are large compared to the wavelength, the modal density is independent of the boundary conditions and the derived formula can be applied for any set of boundary conditions. In fact, the value derived in Ref. [1] equals the input power to an infinite plate.

The procedure in Ref. [1] is commonly used in SEA. However, the derivation considers a homogenous structure. For such structures, the ratio of the averaged square of the modal force to the averaged modal mass equals the ratio of squared force to total mass, which is not generally true. In practical applications of SEA, the expression for homogenous structures is, nevertheless, often used also for inhomogeneous structures. It is then assumed that the force intensity is proportional to the mass density [5].

Another source of error, when using the simple expression in Ref. [1], is peculiar to long structures that support a small number of wave types. Most often, as the frequency is increased, yet another wave type starts to propagate at its 'cut-on' frequency. The modal density increases largely at this frequency, as does the injected power. However, the mobility increases already below the cut-on frequency and, if the structure dissipates energy, so does the injected power, in contrast to the modal density. Thus, the proportionality between injected power and modal density does not apply. This phenomenon is illustrated in Ref. [6] for a fluid-filled pipe, where, for 1% damping, the simple formula give rise to errors of 3–5 dB in third octave bands just below the cut-on frequencies.

In an alternative formulation, Langley calculates the input power to infinitely long structures that support wave motion described by one response variable [7]. The input power is expressed by the waves' dispersion characteristics and it attributes dissipative effects.

In what follows, the modal procedure for the evaluation of input power in Ref. [1] and the wave-based procedure in Ref. [7] are extended to apply also for structures that support many kinds of waves. The presented formulation applies to waveguide structures that have uniform properties along one direction while it may have quite arbitrary, non-uniform, cross-sections. The force is concentrated at a random location along the waveguide but is otherwise arbitrary. The equations of motion are a set of coupled one-dimensional wave equations. Here, these are devised by the waveguide FEM.

Previously, this method has been used, e.g., for studies of vibration in rods with arbitrary cross-section [8]; composite plates [9]; thin-walled beams [10]; railway track [11]; rib-stiffened plates [12]; twisted beams [13]; anisotropic solids [14,15]; conical shells [16], car tyres [17], fluid-filled pipe bends, [18] and a wind tunnel [19]. Possibly, the methods for the evaluation of input power presented here will apply to any structure built up by the elements presented in Refs. [8–19].

The outline of the paper is as follows. Section 2 gives a brief overview of the waveguide finite element method (FEM) and demonstrates its application to a stiffener in a railway car structure. Section 3 develops the generalisation of the methods in Refs. [1,7] for waveguides. The methods are compared and it is shown that in the limit of zero damping they are identical. Finally, in Section 4, the developed procedure is demonstrated for the railway car structure and the results are compared with measurements, showing a fair agreement.

## 2. Waveguide finite elements

### 2.1. Variational statement

Hamilton's principle states that the true motion of a structure minimises the time integral of the difference between strain and kinetic energy minus the work from external forces. Considering harmonic motion of the form $e^{-i\omega t}$, where $\omega$ is angular frequency and $t$ is time, and applying Parceval's identity, the following functional is stationary for true motion

$$H = \int \int (\varepsilon^{*\mathrm{T}} \mathbf{C} \varepsilon - \omega^2 \mathbf{u}^{*\mathrm{T}} \mathbf{m} \mathbf{u} - \mathbf{F}^{*\mathrm{T}} \mathbf{u} - \mathbf{u}^{*\mathrm{T}} \mathbf{F}) \, \mathrm{d}V \, \mathrm{d}\omega, \tag{1}$$

where upper indices * and T denote complex conjugate and vector transpose and $V$ is the structure's domain, $\varepsilon$ is the strain, $\mathbf{u}$ is the displacement and $\mathbf{F}$ is the force. Moreover, $\mathbf{C}$ is the rigidity matrix and $\mathbf{m}$ is the mass matrix, both possibly dependent on location. From reciprocity it follows that they are symmetric matrices. The mass matrix is positive definite and the rigidity matrix is positive definite or positive semi-definite.

For linear motion, the strain is a linear functional of the displacement and thus functional (1) is a symmetric bi-linear functional of the displacement and its conjugate.

Now, Hamilton's principle does not apply for non-conservative motion. A dodge proposed in Ref. [20, Chapter 3], and used, e.g., in Refs. [21–22], is therefore applied in the following. Thus, functional (1), of the displacement and the complex conjugate of the displacement, is replaced with the same symmetric bi-linear functional of the displacement and the complex conjugate of the displacement in an adjoint, mathematically designed, system. This adjoint system is similar to the system under investigation but has negative damping. Also, for linear motion, different frequencies are independent and, for simplicity, one frequency at a time is considered. The resulting functional, here denoted the Lagrangian, is given by

$$L = \int (\varepsilon^{a\mathrm{T}}\mathbf{C}\varepsilon - \omega^2\mathbf{u}^{a\mathrm{T}}\mathbf{m}\mathbf{u} - \mathbf{F}^{*\mathrm{T}}\mathbf{u} - \mathbf{u}^{a\mathrm{T}}\mathbf{F})\,\mathrm{d}V, \tag{2}$$

where the upper index, '$a$', denotes the complex conjugate of the adjoint variable. In the Lagrangian, damping is attributed if the imaginary part of the rigidity matrix is negative (semi) definite. In the absence of damping, the adjoint system is identical to the system and the integral of the Lagrangian over frequency is identical to functional (1).

Lagrangian (2) is stationary for true motion, subject to the boundary conditions, and is taken as the basis for the finite element (FE) formulation in the next section.

### 2.2. Waveguide finite element formulation

Consider a structure that has uniform geometrical and material properties along one direction and define a coordinate system with the $z$-axis along the structure and the $x$- and $y$-axis in the plane of the cross-section. An example of such a structure is the beam in Fig. 1. Note, however, the corrugated plate on which the beam is attached cannot be included in the analysis, since its geometry varies in the $z$-direction.

The structure is sub divided into elements, which have finite dimensions on the cross-section and extends along the $z$-axis. For each element, the rigidity and mass matrix are identified and the strain vector is defined as a function of the displacement. Thus, the Lagrangian is given by the sum of the sub Lagrangians defined for each element.

Within the elements the displacement's dependence of the $x$- and $y$-coordinate is expressed with conventional, polynomial, FE shape functions. Thus, the displacement is given by

$$\mathbf{u}(x,y,z) = \mathbf{\Psi}^{\mathrm{T}}(x,y)\mathbf{v}(z), \quad \mathbf{u}^a(x,y,z) = \mathbf{\Psi}^{\mathrm{T}}(x,y)\mathbf{v}^a(z), \tag{3}$$

where the entries to $\mathbf{\Psi}$ are FE shape functions, which are non-zero within one element only, and $\mathbf{v}$ and $\mathbf{v}^a$ contain the 'nodal' displacements, i.e., the displacements along a line in the $z$-direction. Displacements (3) are inserted into the sub-Lagrangians and the derivatives and integrals with respect to $x$ and $y$ are evaluated. Finally, the sub-Lagrangians are assembled according to standard FE procedures, upon which it follows that

$$L = \int \left( \sum_{n=0}^{2} \sum_{m=0}^{2} \left( \frac{\partial^n \mathbf{v}^{a\mathrm{T}}}{\partial z^n} \mathbf{A}_{nm} \frac{\partial^m \mathbf{v}}{\partial z^m} \right) \left( -\omega^2 \mathbf{v}^{a\mathrm{T}}\mathbf{M}\mathbf{v} - \mathbf{v}^{\mathrm{T}}\mathbf{f}^* - \mathbf{v}^{a\mathrm{T}}\mathbf{f} \right) \mathrm{d}z \right), \tag{4}$$

where $\mathbf{A}_{nm}$ are generalised stiffness matrices, $\mathbf{M}$ is the mass matrix and $\mathbf{f}$ is a generalised force vector. From the properties of the elements' mass matrices it follows that the mass matrix, $\mathbf{M}$, is symmetric and that its real part

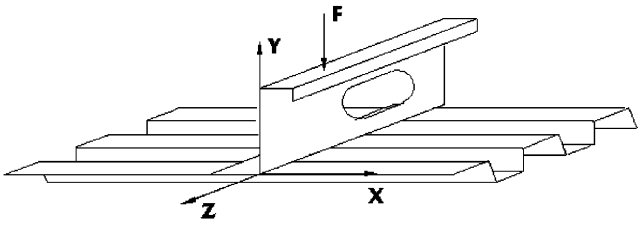


Fig. 1. Sketch of beam and corrugated plate.

is positive definite. Also,

$$\mathbf{A}_{nm} = \mathbf{A}_{mn}^{\mathrm{T}} \tag{5}$$

since the rigidity matrices are symmetric.

The literature describes various elements that may be used in the analysis presented above, see, e.g., Refs. [5–19]. The examples presented in the present work, uses the thin-walled element presented in Ref. [19]. It is equal to Gavric's thin-walled element, except that the transformation to real-valued matrices, given by Ref. [10, Eq. (5)], is not made.

### 2.3. Wave equation

From the calculus of variation applied on Eq. (4), see e.g. Ref. [20], follows the equation of motion

$$\sum_n \mathbf{K}_n \frac{\partial^n \mathbf{v}}{\partial z^n} - \omega^2 \mathbf{M}\mathbf{v} = \mathbf{f}, \tag{6}$$

where

$$\mathbf{K}_n = \sum_{m=0}^{2} ((-1)^{n-m} \mathbf{A}_{(n-m)m}), \quad m \leqslant n \leqslant 4. \tag{7}$$

It follows from Eq. (5) that $\mathbf{K}_n$ is symmetric if $n$ is an even number and anti-symmetric otherwise. Eq. (6) constitutes a set of ordinary linear differential equations with constant coefficients. If there are no external forces, the solutions are exponential functions of the form of

$$\mathbf{v} = \boldsymbol{\varphi} \mathrm{e}^{\mathrm{i}\kappa z} \tag{8}$$

and a twin-parameter eigenvalue problem in $\kappa$ and $\omega$ follows:

$$(\mathbf{K}(\kappa) - \omega^2 \mathbf{M})\boldsymbol{\varphi} = 0, \tag{9}$$

where

$$\mathbf{K}(\kappa) = \sum_n (\mathrm{i}\kappa)^n \mathbf{K}_n. \tag{10}$$

Without dissipative losses and considering real $\kappa$, the stiffness matrix $\mathbf{K}$ is Hermitian and positive semi definite, which follows from Eqs. (5) and (7) and the properties of the rigidity matrix.

Eq. (9) can be solved as a polynomial eigenvalue problem in the wavenumber $\kappa$ for a given frequency, $\omega$. Without dissipative losses, an eigenvalue may be real, in which case it describes a propagating wave. It can also be imaginary or complex, describing strictly decaying or oscillating and decaying, near field, solutions. With losses, the motion always decays away from the sources and there are no real valued wavenumbers. The latter is most easily demonstrated for a system that is proportionally damped, for which the wave solutions are found from the following eigenvalue problem:

$$(1 - \mathrm{i}\eta)\mathbf{K}(\kappa)\boldsymbol{\varphi} - \omega^2 \mathbf{M}\boldsymbol{\varphi} = 0, \tag{11}$$

which is equally written

$$\mathbf{K}(\kappa)\boldsymbol{\varphi} - \lambda \mathbf{M}\boldsymbol{\varphi} = 0, \tag{12}$$

$$\lambda = \omega^2/(1 - \mathrm{i}\eta) \approx \omega^2(1 + \mathrm{i}\eta), \tag{13}$$

where the last approximate equality is valid for small levels of damping. Now, suppose that $\kappa$ is real, then $\mathbf{K}(\kappa)$ is Hermitian and since $\mathbf{M}$ is real, symmetric and positive definite, it follows that the eigenvalue $\lambda$ is real. According to Eq. (13), however, $\lambda$ is a complex number for a given frequency $\omega$. Since this is clearly a contradiction, it is concluded that the wavenumbers $\kappa$ are complex for a damped system. This also shows that an evolution of the wavenumber with frequency, $\kappa(\omega)$, is bound to either the upper or lower complex half-plane.

Symmetry between waves travelling to the left and to the right indicates another important property of the eigenvalue problem (9). If $\kappa_j$ is an eigenvalue to the equation for a given frequency $\omega$, so is $-\kappa_j$, since $\mathbf{M}$ is symmetric and

$$\mathbf{K}(-\kappa_j) = \mathbf{K}(\kappa_j)^{\mathrm{T}}. \tag{14}$$

which follows from Eqs. (7) and (10). Thus, a wave component that propagates or decays in the positive $z$-direction has a left eigenvector, which equals the right eigenvector of a similar component in the negative $z$-direction.

For undamped systems, symmetry exists between wavenumbers in all four quadrants in the complex plane, see Fig. 2. These symmetries, which can be shown by combinations of transposes and complex conjugates together with the Hermitian properties of the matrices in Eq. (9), are summarised in Table 1.

For studies of propagating waves in un-damped structures, the wavenumbers takes real values only. Eq. (9) can then, alternatively, be solved as a generalised linear eigenvalue problem in $\omega$ for a given $\kappa$. The linear problem is smaller than the polynomial and also it is on an efficient form, as the mass matrix is symmetric and positive definite and the stiffness matrix is Hermitian and positive semi-definite. Hence, numerical speed and stability is gained; typically, the calculation burden is reduced by a factor of 100. However, the choice between the polynomial eigenvalue problem in $\kappa$ and the linear eigenvalue problem in $\omega$ is a matter of objectives and both are used in the following analysis of input power to waveguide structures.

### 2.4. Example

To illustrate the discussion above, the beam structure in Fig. 1 is considered. This beam is attached to the base frame of the railway car section shown in Fig. 3. (The section is a full-scale experimental prototype built during the design of a new coach for the Stockholm metro some years ago.) The beam is made of steel and has a wall thickness of 4 mm. The mesh used for the waveguide FE model of the beam is shown in Fig. 4. This model neglects the holes in the beam shown in Figs. 1 and 3, which obviously is an approximation. The

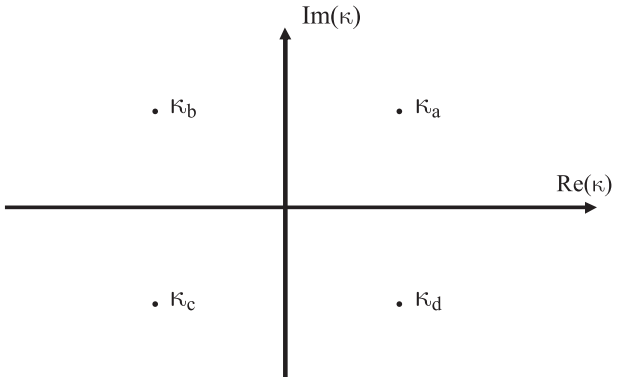


Fig. 2. Symmetry of complex wavenumbers for an undamped structure.

Table 1
Relations between eigenwavenumbers and eigenvectors in different quadrants for undamped waveguides

| Quadrant | Index | Wavenumber (poles) | Right eigenvector | Left eigenvector |
|---|---|---|---|---|
| 1st | a | $\kappa_a$ | $\boldsymbol{\varphi}_a$ | $\boldsymbol{\theta}_a = \boldsymbol{\varphi}_a^*$ |
| 2nd | b | $\kappa_b = -\kappa_a^*$ | $\boldsymbol{\varphi}_b = \boldsymbol{\varphi}_a^*$ | $\boldsymbol{\theta}_b = \boldsymbol{\varphi}_a$ |
| 3rd | c | $\kappa_c = -\kappa_a$ | $\boldsymbol{\varphi}_c = \boldsymbol{\varphi}_a$ | $\boldsymbol{\theta}_c = \boldsymbol{\varphi}_a^*$ |
| 4th | d | $\kappa_d = -\kappa_a^*$ | $\boldsymbol{\varphi}_d = \boldsymbol{\varphi}_a^*$ | $\boldsymbol{\theta}_d = \boldsymbol{\varphi}_a$ |

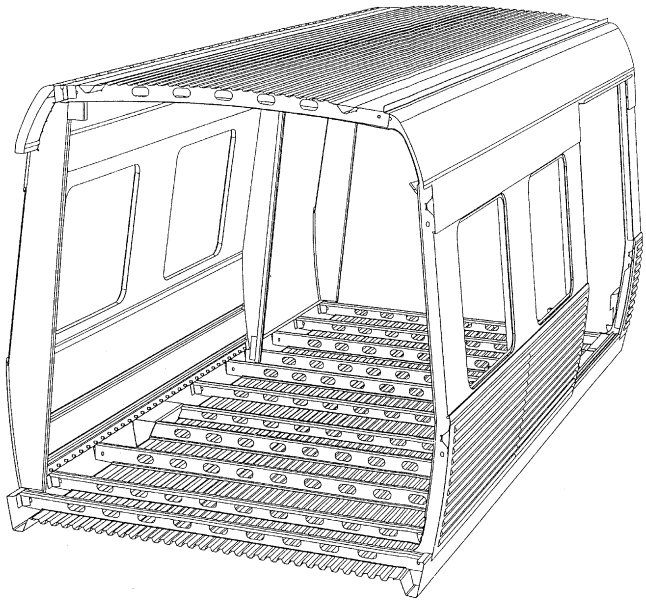

Fig. 3. Sketch of the considered railway car section. The measurements are taken on the second beam from the near end.

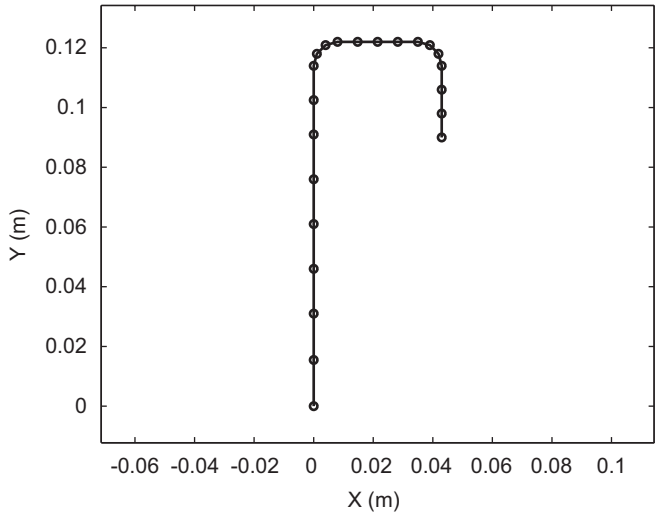


Fig. 4. Waveguide FE mesh of beam. Circles indicate the node location.

corrugated plate cannot be included into the waveguide FE model, since its geometry varies along the beam. Therefore, simplifying boundary conditions are assumed at the connection between the beam and the plate. These boundary conditions are chosen based on the following reasoning.

First, the plate stiffness across the corrugation is very low and hence the axial motion of the beam is assumed to be free. Second, the rotation about the beam axis, i.e., the $z$-axis, is assumed blocked, since the rotational rigidity of the open thin-walled beam is low and the flexural stiffness of the plate along the corrugation is in comparison large. Third, the in plane stiffness along the plate corrugation is high compared to the beam's flexural and rotational stiffness and thus the motion along the corrugation is blocked. Fourth, the beam is there to increase the flexural stiffness of the structure, so it is reasonable to assume the motion in the vertical direction free.

Following the second and fourth argument above, the essential boundary conditions at the connection to the corrugated plate are

$$u = 0 \quad \text{and} \quad \phi_z = 0, \tag{15}$$

where $u$ and $\phi_z$ are the displacement in the $x$ direction and the rotation about the $z$-axis. Following the first and third argument, the natural boundary conditions at the connection are

$$\partial w/\partial z = 0 \quad \text{and} \quad \partial v/\partial y = 0, \tag{16}$$

where $v$ and $w$ are the displacements in the $y$ and $z$ directions.

Obviously, these boundary conditions are somewhat simplistic but, as will be shown in Section 4, they result in a reasonably good estimate of the input power to the structure. Furthermore, as also shown in Section 4, the value of the frequency band averaged input power is not critically dependent of the choice, except in a lower frequency regime.

Fig. 5 shows the dispersion characteristics for the beam. For reference, Fig. 5 also shows the wavenumbers for flexural waves in a 4 mm thick steel plate. In the beam, there are two waves propagating at low frequencies, since there are two degrees of freedom that are not restrained by the boundary conditions (15). At increasing frequencies, additional waves are "cut-on". i.e., they start propagating. Normally, the dispersion curves do not cross. An exception is the axial, dilatational, wave, which is dynamically uncoupled from all other waves for the chosen boundary conditions. It is seen as a straight line through most of the other curves in Fig. 5.

In Fig. 5, the dispersion characteristics are shown with dots, each defining a wavenumber and a frequency that constitutes an eigenvalue pair to Eq. (9). It is of interest to sort this collection of dots into branches that define different wave types. At lower frequencies, when there are only a few branches, this is not difficult, while at higher frequencies it becomes increasingly tricky. The problems are illustrated in Figs. 6 and 7. Fig. 6 shows the dispersion curves amplified around the near crossing of two branches and Fig. 7 shows the cross-sectional mode shapes at frequencies just below and above the crossing. Based on the wave shapes in Fig. 7, it would be natural to sort the solutions B and D as belonging to the same branch; however, this would indicate that the dispersion curves cross, which is not the case. Also, the wave shapes for the solutions A and C are not similar. Thus, the proper sorting of the waves is not evident.

An interesting behaviour of the dispersion curves appears if the corners of the beam are modelled as sharp 90° bends. The branch that has a cut-on a little above 7.5 kHz is shown amplified for this case in Fig. 8 and it is seen that the lowest frequency for which the wave propagates is given by a finite wavenumber. At somewhat higher frequencies, the lower part of the branch shows wavenumbers that decrease towards zero with

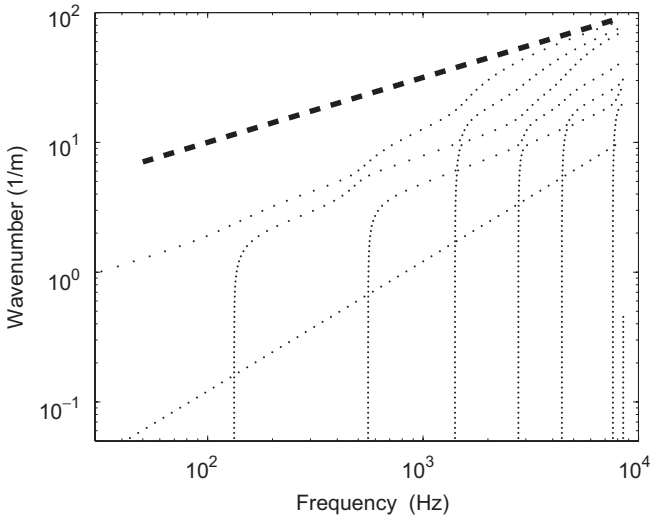


Fig. 5. Dispersion characteristics. Dots, solutions to Eq. (9) for beam; dashed line, steel plate with 4 mm thickness.

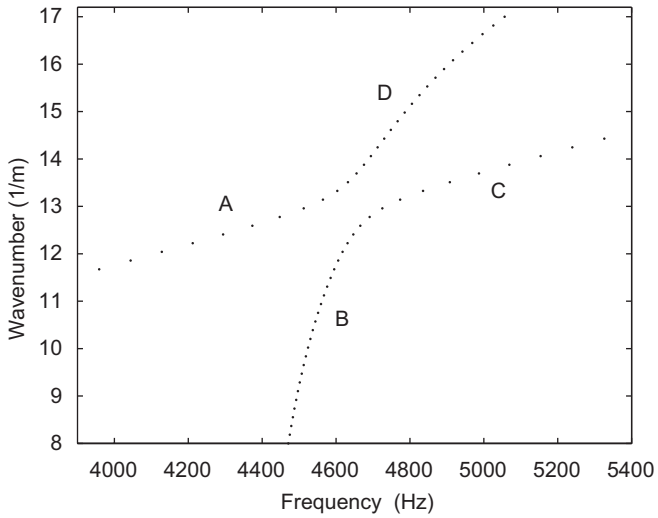


Fig. 6. Magnified dispersion characteristics of beam.

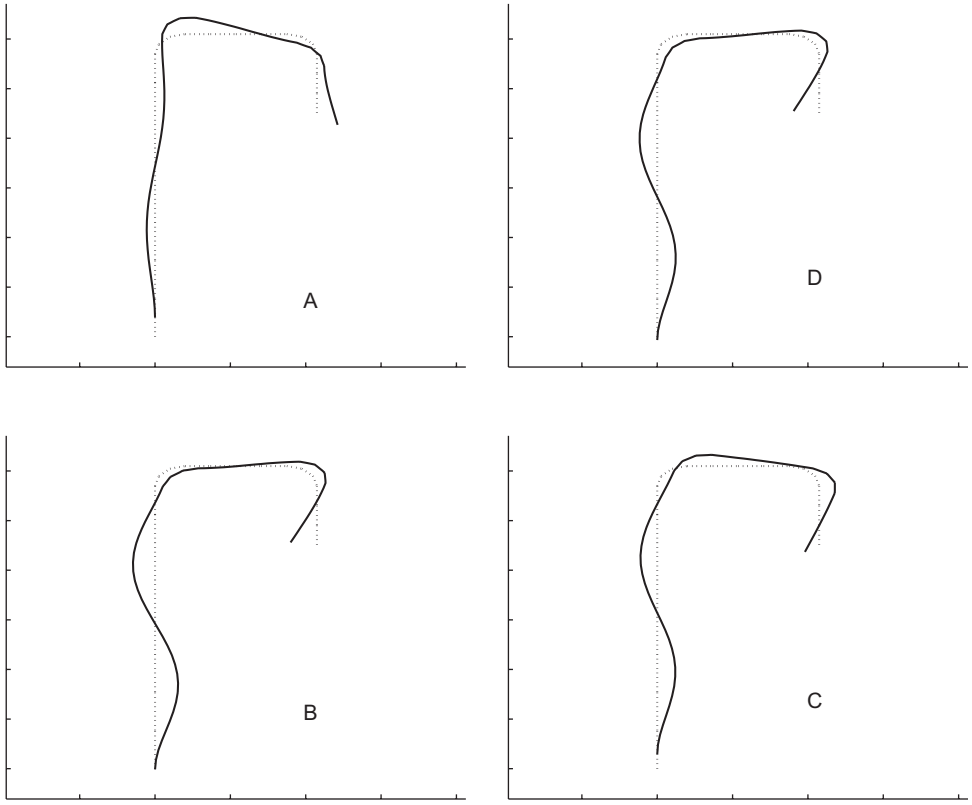


Fig. 7. Wave forms corresponding to dispersion relations in Fig. 6.

increasing frequencies, while the upper part shows wavenumbers that increase with frequency. It follows that for the lower part, the phase velocity and the group velocity are in opposite directions. Such waves have been observed previously, e.g., for cylindrical shells [26] and car tyres [17]. Fig. 9 illustrates the evolution of the complex wavenumber with frequency for a damped and an undamped structure. The form of the observed evolution will have implications for the expressions for input power that are developed in the next section.

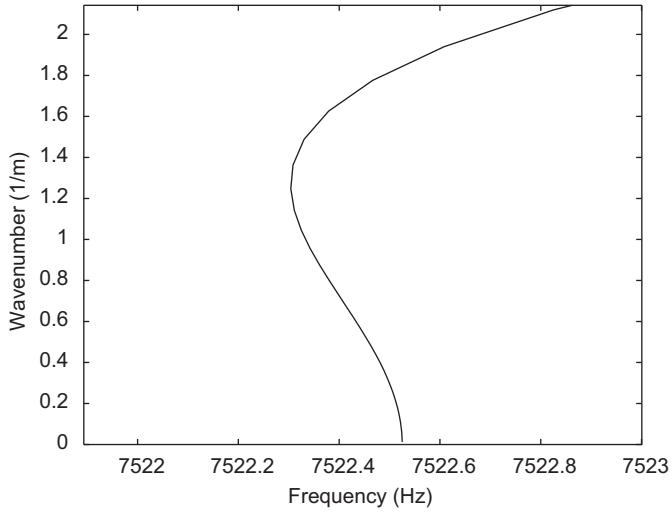


Fig. 8. Dispersion characteristics for the beam modelled with sharp corners, amplified.

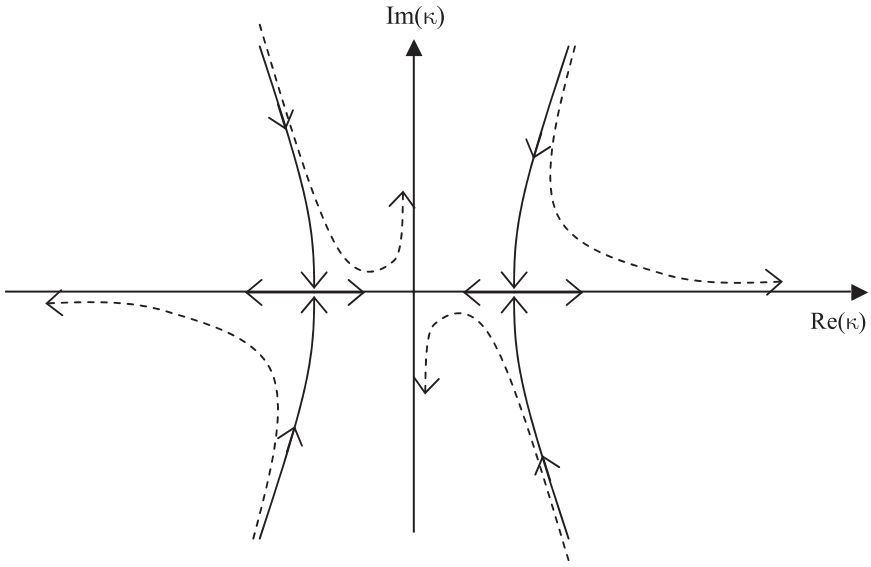


Fig. 9. Evolution with frequency of complex wavenumber. Solid line, undamped structure; dashed line, damped structure.

## 3. Input power to waveguide structures

Two methods are developed for the calculation of input power to waveguide structures in the following. The first is a modal approach, inspired by the calculation of input power to a point loaded simply supported plate in Ref. [1, Chapter IV.4]. The second is a wave approach, expanding Langley's result in Ref. [7] to general waveguides.

### 3.1. The modal approach

Consider a waveguide of length $L$, located at $z \in [0, L]$. It is excited by a harmonic force that is concentrated at location $z_0$ but is otherwise arbitrary. Damping is described as stiffness proportional and the equation of

motion (6) takes the form of

$$(1-\mathrm{i}\eta)\sum_n \mathbf{K}_n \frac{\partial^n \mathbf{v}}{\partial z^n} - \omega^2 \mathbf{M}\mathbf{v} = \mathbf{f}_0 \delta(z-z_0). \tag{17}$$

For structures that are long compared to the wavelength, the frequency averaged input power does not largely depend on the precise boundary conditions at the ends. Therefore, a 'convenient' set of boundary conditions is considered. This convenient set is defined so that if a wave, of the form of Eq. (8), impinges on the boundary, it is reflected but no other wave nor any near field components are generated. For structures built-up by the solid element in Ref. [5] and the thin-walled shell element in Ref. [19], this would be the shear-diaphragm boundary condition where the motion in the plane of the cross-section is blocked while the motion along the waveguide is free.

The solution to Eq. (17) is sought as a linear combination of the undamped modes, obeying the convenient boundary condition. To that end, we consider the homogenous form of the equation for an undamped waveguide. It was shown in Section 2.3 that if $\mathbf{v} = \boldsymbol{\varphi}\mathrm{e}^{\mathrm{i}\kappa z}$ is a solution, so is $\mathbf{v} = \boldsymbol{\varphi}^*\mathrm{e}^{-\mathrm{i}\kappa z}$. Thus,

$$\mathbf{v} = (\boldsymbol{\varphi}\mathrm{e}^{\mathrm{i}\kappa z} + \boldsymbol{\varphi}^*\mathrm{e}^{-\mathrm{i}\kappa z})/2 = \mathrm{Re}(\boldsymbol{\varphi})\cos\kappa z - \mathrm{Im}(\boldsymbol{\varphi})\sin\kappa z \tag{18}$$

is also a solution.

The cross-sectional modes $\boldsymbol{\varphi}$ are normalised so that the real part corresponds to the motion along the waveguide and the imaginary part to the motion in the plane of the cross-section. This is possible for structures built up by isotropic or orthotropic elements, such as the solid element in Ref. [5] and the thin-walled element in Ref. [19]. Thus, if the variational parameters are taken as the displacements in the plane of the cross-section and the displacements along the structure multiplied by minus the imaginary unit, the resulting generalised stiffness matrix $\mathbf{K}(\mathrm{i}\kappa)$, for a real wavenumber $\kappa$, is real and symmetric positive semi definite, as shown by Gavric [10]. The mass matrix $\mathbf{M}$ is real and positive definite and, therefore, the eigenvectors to the generalised eigenvalue problem $(\mathbf{K}-\omega^2\mathbf{M})\boldsymbol{\varphi} = 0$ are real. Consequently, the above mentioned normalisation of the eigenvectors of the original generalised eigenvalue is possible. Similar arguments are used for finite strip elements and axi-symmetric FEs, see for instance [23, Chapters 10.6 and 10.7]. Note, however, these arguments do not hold for general anisotropic media, as also discussed in Refs. [15,23].

From the solution to the equations of motion (18), the proposed normalisation of the cross-sectional modes and the definition of the convenient boundary condition it follows that the structure's eigenmodes $\boldsymbol{\psi}_{pr}$ are given by

$$\boldsymbol{\psi}_{pr}(z) = \cos(\kappa z)\mathrm{Re}(\boldsymbol{\varphi}_{pr}) - \sin(\kappa z)\mathrm{Im}(\boldsymbol{\varphi}_{pr}), \tag{19}$$

where

$$\kappa = p\pi/L. \tag{20}$$

For a given value of $\kappa = p\pi/L$, there are many frequencies that satisfies the homogenous and undamped version of Eq. (17). The lowest of these frequencies is denoted $\omega_{p,1}$ and the corresponding eigen vector is $\boldsymbol{\varphi}_{p,1}$, and so on. Thus, a value of the index $r$ denotes a branch of dispersion curves, such as those in Fig. 5.

The eigenmodes obey the following orthogonality relations:

$$\begin{aligned}\int_0^L (\boldsymbol{\psi}_{qs})^{\mathrm{H}}\mathbf{M}\boldsymbol{\psi}_{pr}\mathrm{d}z &= \delta_{qp}\delta_{sr}m_{pr}L/2,\\ \int_0^L (\boldsymbol{\psi}_{qs})^{\mathrm{H}}\mathbf{K}(\kappa_p)\boldsymbol{\psi}_{pr}\mathrm{d}z &= \delta_{qp}\delta_{sr}\omega_{pr}^2 m_{pr}L/2,\end{aligned} \tag{21}$$

where upper index H denotes complex conjugate and transpose and

$$m_{pr} = \boldsymbol{\varphi}_{pr}^{\mathrm{H}}\mathbf{M}\boldsymbol{\varphi}_{pr}. \tag{22}$$

Upon this basis, the power injected by the force is given by [1]

$$P_{\text{in}} = \frac{1}{2}\text{Re}\left(\sum_p \sum_r \frac{2(-\text{i}\omega)\left|\mathbf{f}_0^{\text{H}}\boldsymbol{\psi}_{pr}(z_0)\right|^2}{Lm_{pr}((1-\text{i}\eta)\omega_{pr}^2-\omega^2)}\right). \tag{23}$$

*3.1.1. Statistical expectation of input power*

In line with standard procedures in SEA [1], the frequency averaged value of the input power (23) is evaluated for a random location of the force

$$\bar{P}_{\text{in}} = \frac{1}{\Delta_\omega L}\int_0^L \int_{\omega_l}^{\omega_u} P_{\text{in}}\,\text{d}\omega\,\text{d}z, \tag{24}$$

where $\Delta_\omega = \omega_u - \omega_l$. It is assumed that the bandwidths of the resonances are small, so that most of the energy associated with a resonance, having its natural frequency within a frequency band, is contained in this band. Yet, the frequency band is so narrow that the cross-sectional mode shape $\boldsymbol{\varphi}_{pr}$, for branch $r$ of the dispersion relations, does not vary much for the modes within the band. Upon this basis, the integrals in Eq. (24) are evaluated as in Ref. [1]:

$$\bar{P}_{\text{in}} = \frac{1}{2}\sum_r \frac{\pi}{2}\frac{\left|\mathbf{f}_0^{\text{H}}\boldsymbol{\varphi}_{pr}\right|^2}{Lm_{pr}}\frac{N_r}{\Delta_\omega}, \tag{25}$$

where $N_r$ is the number of resonances within the frequency band, associated with branch $r$.

The cross-sectional mode shape, $\boldsymbol{\varphi}_{pr}$ is an implicit function of frequency, i.e., it is the mode shape for branch $r$ calculated for the wavenumber at frequency $\omega$. At lower frequencies, when the dispersion relations have only a few branches, it is not difficult to identify these branches and thus to find the cross-sectional mode shape for a certain branch at a given frequency.

An alternative to Eq. (25) that avoids the identification of the branches, useful for waveguides that are not too long, is based on the "exact" mode count

$$\bar{P}_{\text{in}} = \frac{\pi}{4L\Delta_\omega}\sum_r \sum_p \int_{\omega_l}^{\omega_u} \frac{\left|\mathbf{f}_0^{\text{H}}\boldsymbol{\varphi}_{pr}\right|^2}{m_{pr}}\delta(\omega_{pr}-\omega)\,\text{d}\omega. \tag{26}$$

Note, however, the apparent precision in this expression is illusory in most situation where SEA is useful. Instead, asymptotic expressions for the mode count are derived in the next section.

*3.1.2. Mode count*

It follows from Eq. (20) that the mode count $N_r$ is approximately given by

$$N_r \approx (\kappa_r(\omega_u) - \kappa_r(\omega_l))L/\pi \tag{27}$$

provided that $\kappa_r$ is an increasing function of frequency. Sometimes, however, it may be otherwise, as discussed in Section 2.4.

The application of Eq. (27) to the dispersion characteristics shown in Fig. 8 requires that the region, where the wavenumber is a multivalued function of frequency is identified and that the upper and lower parts of the curve are handled separately. Moreover, the mode count associated with the lower part is the absolute value of the one given by the equation.

At higher frequencies, the dispersion relations may be intricate and it might be difficult to identify that two solutions belong to the same branch, which is required for the evaluation of Eq. (27). An alternative is then to estimate the mode count from the following asymptotic expression for the modal density [19]

$$\frac{N_r}{\Delta_\omega} \approx n_r(\omega) \approx \frac{L}{\pi}\left|\frac{\partial\kappa_r}{\partial\omega}\right| = \frac{L}{\pi}\frac{2\omega m_{pr}}{\left|\boldsymbol{\varphi}_{pr}^{\text{H}}\mathbf{K}'\boldsymbol{\varphi}_{pr}\right|}, \tag{28}$$

where $n_r$ is the modal density and

$$\mathbf{K}' = \frac{\partial \mathbf{K}(\kappa_r)}{\partial \kappa_r}. \tag{29}$$

This expression, in contrast to the one in Ref. [19], takes the absolute value of the denominator and therefore it is valid also when the wavenumber is a decreasing function of frequency. The expression can be evaluated by considering one solution to the dispersion relations at a time. It is, however, singular at the cut-on frequencies, which is inferred from the following arguments.

At a cut-on frequency, $\omega \neq 0$, such that the wavenumber $\kappa = 0$, the eigenvector is given by

$$\mathbf{K}_0 \boldsymbol{\varphi} - \omega^2 \mathbf{M} \boldsymbol{\varphi} = 0. \tag{30}$$

This eigenvector is real, since $\mathbf{K}_0$ and $\mathbf{M}$ are real and symmetric. Consequently, the denominator in Eq. (28) is, for $\kappa = 0$,

$$\boldsymbol{\varphi}^{\mathrm{T}}(\mathrm{i}\mathbf{K}_1)\boldsymbol{\varphi} = \boldsymbol{\varphi}^{\mathrm{T}}(-\mathrm{i}\mathbf{K}_1)\boldsymbol{\varphi} = 0, \tag{31}$$

since the transpose of the scalar $\boldsymbol{\varphi}^{\mathrm{T}}(\mathrm{i}\mathbf{K}_1)\boldsymbol{\varphi}$ equals itself and $\mathbf{K}_1$ is an anti-symmetric matrix. A consequence of this result is that the group velocity is zero for $\kappa = 0$, see Ref. [19, Eq. (18)].

In conclusion, a waveguide is excited by a force concentrated at an axial location, as described by Eq. (17). The response is calculated for a set of convenient boundary conditions at the ends and is expressed as a modal sum. Upon this basis, the frequency averaged power injected by a force at a random axial location is given by Eq. (25). In this equation, the mode count may be evaluated, as in Eq. (26), by simply calculating the natural frequencies when the wavenumber is given by Eq. (20). It may also be evaluated by Eq. (27), provided that the regions where the dispersion relation for a branch is a multivalued function of frequency are identified. Finally, it can be estimated from the asymptotic modal density (28), in which case the injected power is given by

$$\bar{P}_{\mathrm{in}} = \sum_r \frac{\omega}{2} \frac{\left|\mathbf{f}_0^{\mathrm{H}} \boldsymbol{\varphi}_{pr}\right|^2}{\left|\boldsymbol{\varphi}_{pr}^{\mathrm{H}} \mathbf{K}' \boldsymbol{\varphi}_{pr}\right|}, \tag{32}$$

where the summation is taken over the branches of the dispersion characteristics. Unfortunately, this expression is singular at the cut-on frequencies.

### 3.2. The wave approach

In this section, the power injected by the force on the right-hand side of Eq. (17) is calculated upon the assumption that the waveguide is infinitely long. This formulation is not singular at the cut-on frequencies, if damping is attributed.

First, a spatial Fourier transform is applied, and the equation becomes

$$\mathbf{D}(\kappa)\tilde{\mathbf{u}}(\kappa) = \tilde{\mathbf{f}}, \tag{33}$$

where

$$\mathbf{D}(\kappa) = (1 - \mathrm{i}\eta) \sum_n (\mathbf{K}_n (\mathrm{i}\kappa)^n) - \omega^2 \mathbf{M}, \tag{34}$$

$$\tilde{\mathbf{u}}(\kappa) = \int_{-\infty}^{\infty} \mathbf{u}(z) \mathrm{e}^{-\mathrm{i}\kappa z} \, \mathrm{d}z, \quad \tilde{\mathbf{f}}(\kappa) = \int_{-\infty}^{\infty} \mathbf{f}(z) \mathrm{e}^{-\mathrm{i}\kappa z} \, \mathrm{d}z = \mathbf{f}_0 \mathrm{e}^{-\mathrm{i}\kappa z_0}. \tag{35}$$

The input power to the structure is given by

$$P_{\mathrm{in}} = \frac{1}{2} \mathrm{Re}\left(\mathbf{f}_0^{\mathrm{H}}(-\mathrm{i}\omega \mathbf{u}(z = z_0))\right) = \frac{1}{4\pi} \mathrm{Re}\left(\mathbf{f}_0^{\mathrm{H}} \lim_{z \to +z_0} \int_{-\infty}^{\infty} -\mathrm{i}\omega \tilde{\mathbf{u}}(\kappa) \mathrm{e}^{\mathrm{i}\kappa z} \, \mathrm{d}\kappa\right). \tag{36}$$

The integral appearing on the right-hand side of this expression is evaluated by contour integration; the contour chosen here consists of the real axis together with a semi-circle enclosing the upper half-plane. The poles and residues are identified by a theorem from Ref. [24], which is repeated for completeness.

**Theorem.** *Let the elements of a square matrix* $\mathbf{D}(\kappa)$ *and a column vector* $\tilde{\mathbf{f}}(\kappa)$ *be analytic functions of* $\kappa$ *in a neighbourhood of a simple zero* $\kappa_j$ *of det* $(\mathbf{D}(\kappa))$ *and let* $\tilde{\mathbf{u}}(\kappa)$ *be the solution to Eq.* (33). *Then* $(\kappa-\kappa_j)\ \tilde{\mathbf{u}}(\kappa)$ *is analytic in a neighbourhood of* $\kappa_j$ *and*

$$\lim_{\kappa\to\kappa_j}(\kappa-\kappa_j)\tilde{\mathbf{u}}(\kappa)=\frac{\boldsymbol{\theta}_j^{\mathrm{T}}\tilde{\mathbf{f}}(\kappa)}{\boldsymbol{\theta}_j^{\mathrm{T}}\mathbf{D}'(\kappa_j)\boldsymbol{\varphi}_j}\boldsymbol{\varphi}_j, \tag{37}$$

*where the non-zero vectors* $\boldsymbol{\theta}_j$ *and* $\boldsymbol{\varphi}_j$ *are determined uniquely, apart from scalar factors, by*

$$\mathbf{D}(\kappa_j)\boldsymbol{\varphi}_j=0,\quad \mathbf{D}(\kappa_j)^{\mathrm{T}}\boldsymbol{\theta}_j=0. \tag{38}$$

The assumptions of the theorem ensure that the denominator of the right-hand side of Eq. (37) is non-zero. For an undamped structure, however, there is a double pole at the cut-on, as seen in Fig. 9, and the expression is singular. Also, the restriction of a simple pole is violated for waveguides with cross-sections having two axes of symmetry, for instance circular or quadratic waveguides. However, since the eigenvectors for such double poles are linearly independent, Eq. (37) still holds, see Ref. [25].

The poles required for the evaluation of the integral in Eq. (36) are thus identified by the theorem and it follows that

$$P_{\mathrm{in}}=\frac{\omega}{2}\sum_{\mathrm{Im}\,(\kappa_j>0)}\mathrm{Re}\left(\frac{(\boldsymbol{\theta}_j^{\mathrm{T}}\mathbf{f}_0)(\mathbf{f}_0^{\mathrm{H}}\boldsymbol{\varphi}_j)}{\boldsymbol{\theta}_j^{\mathrm{T}}\mathbf{D}'(\kappa_j)\boldsymbol{\varphi}_j}\right), \tag{39}$$

where the poles $\kappa_j$ and the left and right eigenvectors, $\boldsymbol{\varphi}_j$ and $\boldsymbol{\theta}_j$, are given by the solutions to the polynomial eigenvalue problem, defined by Eqs. (34) and (38) for a given frequency $\omega$. This expression will predict a finite input power at the cut-on frequencies, if damping is attributed. It is a generalisation of the result in Ref. [7] to systems with multidimensional dispersion characteristics and constitutes the major result of the present study. It should be useful as the waveguide FEM is a versatile tool that may be applied to virtually any structure that has constant properties along one direction.

### 3.3. Input power to an infinite waveguide without damping

It is of interest to compare the wave expression for input power (39) to the modal expression (25). To that end, Eq. (33) is considered for a structure without damping. As shown in Appendix A, for such structures, waves associated with poles that have non-zero imaginary parts do not receive any input power. Consequently, it is only the poles on the real axis that need be included in the summation (39). Moreover, it is only poles associated with the upper half-plane that should be included. To identify these, the wavenumber is considered for a lightly damped structure

$$\kappa=\kappa_0+\frac{\partial\kappa}{\partial\eta}\eta, \tag{40}$$

where $\kappa$ is a solution to Eq. (12) and $\kappa_0$ is the associated real solution found in the limit of zero damping. The derivative above should also be evaluated in this limit. To that end, the derivative of Eq. (12) with respect to $\eta$ is taken

$$\frac{\partial}{\partial\eta}((\mathbf{K}(\kappa)-\omega^2(1+\mathrm{i}\eta)\mathbf{M})\boldsymbol{\varphi})=\left(\mathbf{K}'(\kappa)\frac{\partial\kappa}{\partial\eta}-\mathrm{i}\omega^2\mathbf{M}\right)\boldsymbol{\varphi}+(\mathbf{K}(\kappa)-\omega^2(1+\mathrm{i}\eta)\mathbf{M})\frac{\partial\boldsymbol{\varphi}}{\partial\eta}=0. \tag{41}$$

This equation is pre multiplied with the left eigenvector, which for a propagating wave in a system without damping is the complex conjugate of the right eigenvector. The resulting expression is rearranged, and it

follows that

$$\frac{\partial\kappa}{\partial\eta}=\frac{\mathrm{i}\omega^2\boldsymbol{\varphi}^{\mathrm{H}}\mathbf{M}\boldsymbol{\varphi}}{\boldsymbol{\varphi}^{\mathrm{H}}\mathbf{K}'(\kappa)\boldsymbol{\varphi}}=\frac{\mathrm{i}\omega}{2c_g}, \tag{42}$$

where the group velocity $c_g$ for an undamped waveguide is given by [19]

$$c_g=\frac{\partial\omega}{\partial\kappa}=\frac{\varphi^{\mathrm{H}}\mathbf{K}'(\kappa)\varphi}{2\omega\varphi^{\mathrm{H}}\mathbf{M}\varphi}. \tag{43}$$

It follows from Eqs. (40) and (42) that waves having a positive group velocity are associated with the upper complex plane and should be included in the summation (39). Thus, the input power to an undamped infinite waveguide is given by

$$P_{\mathrm{in}}=\frac{\omega}{2}\sum_{c_{gj}>0,\,\mathrm{Im}\,(\kappa_j=0)}\frac{\left|\boldsymbol{\varphi}_j^{\mathrm{H}}\mathbf{f}_0\right|^2}{\boldsymbol{\varphi}_j^{\mathrm{H}}\mathbf{K}'(\kappa_j)\boldsymbol{\varphi}_j}, \tag{44}$$

where it is noted that the denominator is a real and positive quantity for each term.

In Section 2, it was seen that if $\kappa$ is a solution to the dispersion relations, so is $-\kappa$. From reasons of symmetry it follows that one of these solutions is associated with a positive and the other with a negative group velocity of the same magnitude. Thus, the summation in Eq. (44) is equally made for the positive real wavenumbers, if the absolute value of the denominator is considered.

In conclusion, expression (39) for the input power to an infinite waveguide equals Eq. (32). Thus, the asymptotic modal approach and the wave approach estimate the injected power equally, if the structure has no damping.

Finally, it is worth noting that, in a similar analysis, Langley draws the erroneous conclusion that it is the waves with a positive wavenumber that are associated with the upper complex half-plane [7, p. 659]. Thus, an equation similar to Eq. (32) results, except that it will predict a negative input power for waves that have phase velocity and group velocity in different directions.

## 4. Input power to a railway car structure

To demonstrate the formulation derived above, the vibrational power injected by a point force on the beam in Fig. 2 was measured. Thus, a shaker excited a force in the vertical direction at the middle of the top flange,

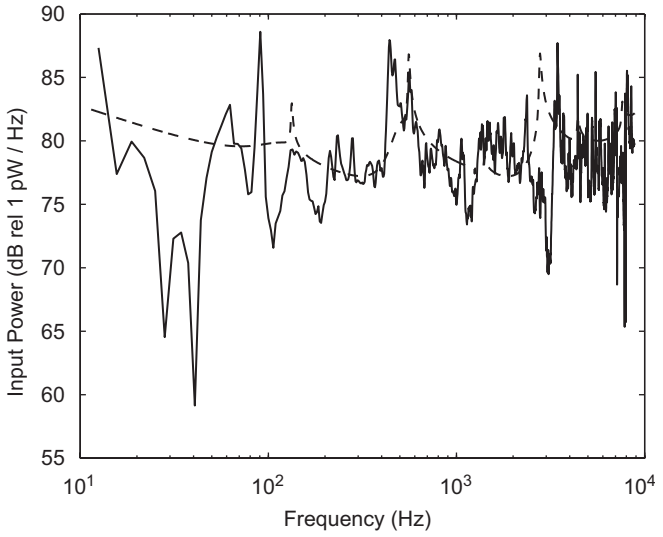


Fig. 10. Input power to railway car structure. Solid line, measured; dashed line, calculated with Eq. (39).

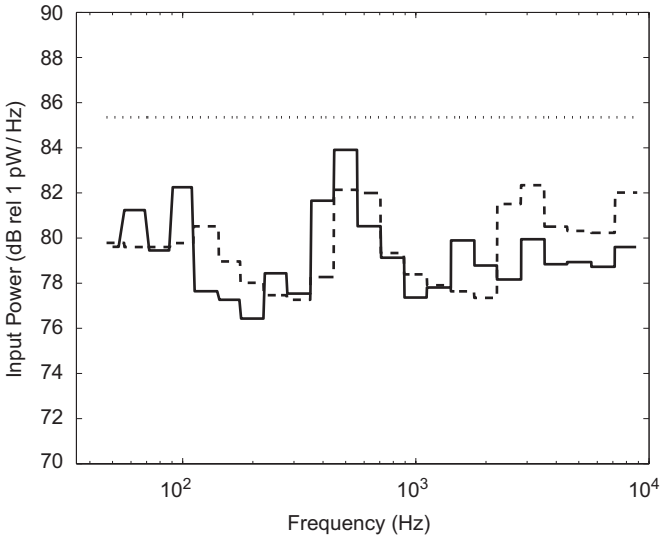


Fig. 11. Input power to railway car structure. Solid line, measured; dashed line, calculated with Eq. (39); dotted line, SEA estimate for a 4 mm steel plate.

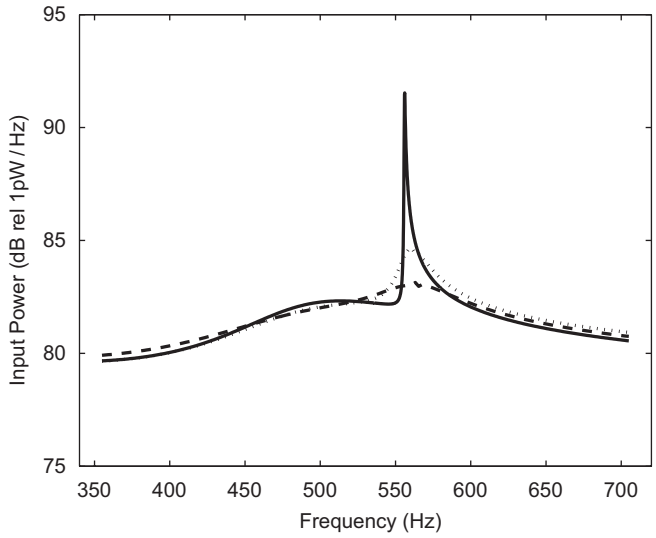


Fig. 12. Input power. Solid line, $\eta = 0.001$; dashed line, $\eta = 0.1$; dotted line, $\eta = 0.001$ except for top flange where $\eta = 0.2$.

at the location $(x, y) = (0.028, 0.12)$, see Fig. 3. The force and the response of the beam were measured with a Brüel & Kjaer 8001 impedance head.

Fig. 10 shows the input power injected by a force of unit magnitude in narrow bands, while Fig. 11 shows the same result in third-octave bands. For reference, Fig. 11 shows also the SEA estimate of the input power to a 4 mm steel plate. This is the value that many SEA practitioners would choose for a high-frequency estimate of the input power, in the lack of alternatives.

Damping is modelled with a hysteretic damping loss factor and its level was guessed, $\eta = 0.02$; this being a typical value for rather complex welded steel structure [1, p. 238]. At lower frequencies, the beam's length has a major influence on the results and the predicted value is greatly in error. From 50 Hz, however, the prediction is of the correct order of magnitude and for 23 consecutive third-octaves, from 50 Hz to 8 kHz, the values predicted by Eq. (39) agree with the measured values, with an error that is less than 3.5 dB.

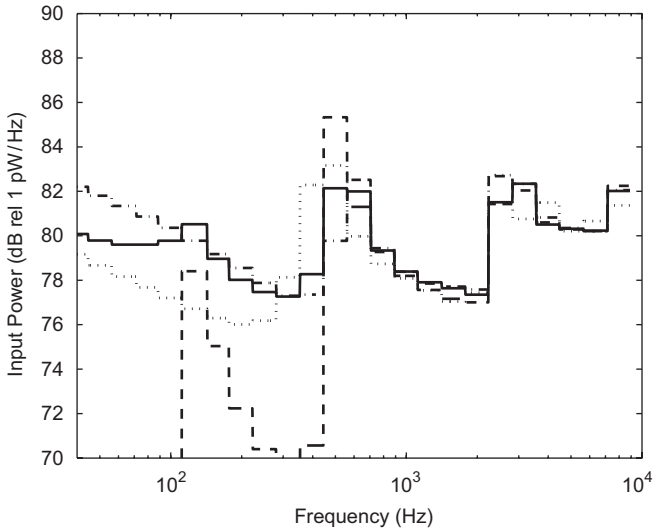


Fig. 13. Calculated input power to railway car structure for different boundary conditions at the corrugated plate. Solid line, considered boundary conditions; dashed line, blocked condition; dotted line, shear diaphragm condition; dash–dot line, free condition.

If the dispersion characteristics in Fig. 5 are compared to the calculated input power in Fig. 10, it is seen that the input power has maxima at the cut-on frequencies around 130, 550 Hz and 2.8 kHz. The cut-on around 1.4 kHz, however, is not quite evident in the input power, since this wave form has a nodal line at the cross-sectional coordinate where the force acts. Comparing the measured and calculated values in Fig. 10, it appears as if the cut-on frequencies at 130 and 550 Hz are over estimated, while the one at 2.8 kHz is under estimated.

Fig. 12 shows the influence of damping on the results. Thus, the results for a hysteretic damping of magnitude $\eta = 0.001$ are compared to those for $\eta = 0.1$. Much of the theoretical analysis above consider structures that are proportionally damped; Eq. (39), however, applies equally for structures that have an arbitrary distribution of damping. To illustrate the results for such a structure, Fig. 12 shows also the results when the top flange has an added damping, $\eta = 0.2$, while the rest of the beam has a very low level of damping, $\eta = 0.001$. It appears as if, at the considered frequencies, the damping material is perhaps better used if it is evenly distributed.

The results presented above are calculated for a set of simple boundary conditions at the connection between the beam and the corrugated plate. The choice was based on an "educated guess" in Section 2.4 and it was claimed that it was not critical. This statement is substantiated in Fig. 13, showing the results for: a, the considered boundary condition, $u = \phi_z = 0$; b, blocked condition, $u = v = w = \phi_z = 0$; c, shear diaphragm condition, $u = w = 0$ and d, free condition, where it is understood that a non-restricted degree of freedom is not impeded by any boundary force.

The blocked condition is special in that there are no waves propagating in the structure at lower frequencies and, consequently, the injected power is very low. Other than that, the injected power is quite indifferent to the chosen boundary condition.

## 5. Conclusions

This paper considers the power injected into waveguide structures from forces that are concentrated along the waveguide but are otherwise arbitrary. The derived formulation should be particularly useful for an SEA. The motion of the structure is described by a set of coupled, linear, one-dimensional wave equations. These equations are, in this work, devised by the waveguide FEM, which is a versatile tool for describing wave motion in general structures that have uniform properties along one direction. Possibly, the methods for the evaluation of input power presented here will apply to any structure built up by the elements presented in the Refs. [5–19].

SEA may be conceived in a modal approach or a wave approach and in line with this there are in the literature a modal and a wave formulation for the evaluation of input power. The application of these formulations to structures described by the waveguide FEM is developed in this work.

First, the modal formulation in Ref. [1] is applied for general finite length waveguide structures. The WFEM allows an efficient identification of the modes and natural frequencies for a convenient set of boundary conditions at the ends. Upon this basis the injected power is expressed by a modal summation and then frequency averaged as in Ref. [1]. The resulting expression is proportional to the modal density and to the ratio of squared modal force to modal mass, which are explicitly identified.

Second, an infinite waveguide is considered and the derivation in Ref. [7] is expanded to apply also for multidimensional dispersion relations. The input power is given by an inverse Fourier transform, which is solved by residue calculus. The poles describe the damped wave solution and are given by a polynomial eigenvalue problem. This procedure is numerically more costly; however, it attributes damping effects and avoids some difficulties in the modal procedure.

The modal procedure requires the modal density, which may be identified by a direct mode count, for a structure obeying convenient boundary conditions. It can also be evaluated by the asymptotic expressions (27) and (28). In doing this, care must be taken whenever a wave has its group and phase velocity in different directions, in which case the wavenumber is a decreasing function of frequency. This fact seems to have been overlooked in the past, e.g., Ref. [19].

Another complication appears for waveguides at the cut-on frequencies, where the asymptotic modal density becomes infinite. A good solution for the handling of this singularity has not appeared and it seems as the modal approach based on the asymptotic modal density is quite useless whenever a cut-on frequency is encountered.

A waveguide FE model of a stiffener in a railway-car structure serves as a demonstration example of the method. Calculation of the input power from a point force is subsequently made using the wave approach. The results are compared with an in situ measurement made on a full scale railway car section. The results agree within 3.5 dB for the third octave bands from 50 Hz to 8 kHz. This level of accuracy is often sufficient and considering the ease by which the model is made, the presented procedures should be useful whenever the power input to waveguide structures is of interest.

## Acknowledgement

The financial support by the Swedish Research Council for Engineering Science is gratefully acknowledged.

## Appendix A

For a structure without damping, the near field solutions cannot absorb any energy nor transport energy away from the excitation and, hence, there is no contribution to the input power (39) associated with imaginary or complex poles. For completeness, this is demonstrated in what follows.

For an imaginary pole, $\mathrm{Im}\{\kappa_j\}>0$ and $\mathrm{Re}\{\kappa_j\}=0$, $\mathbf{K}(\kappa_j)$ is real and $\mathbf{K}'(\kappa_j)=\mathbf{D}'(\kappa_j)$ is imaginary. The eigenvectors, $\boldsymbol{\varphi}_j$ and $\boldsymbol{\theta}_j$, given by Eq. (38), are the column null-spaces of the real matrices $\mathbf{D}(\kappa_j)$ and $\mathbf{D}(\kappa_j)^{\mathrm{T}}$, respectively. Consequently, $\boldsymbol{\varphi}_j$ and $\boldsymbol{\theta}_j$ are real-valued vectors. The input power,

$$P_{\mathrm{in},j}=\frac{\omega}{2}\mathrm{Re}\left(\frac{\boldsymbol{\theta}_j^{\mathrm{T}}\mathbf{f}_0\mathbf{f}_0^{\mathrm{H}}\boldsymbol{\varphi}_j}{\boldsymbol{\theta}_j^{\mathrm{T}}\mathbf{D}'(\kappa_j)\boldsymbol{\varphi}_j}\right)$$

is thus zero, since the bracketed expression is imaginary.

Complex poles appear in quadruples, see Table 1. Of the four poles, $\kappa_a=\kappa_j$ and $\kappa_b=\kappa_j^*$, belongs to the upper half-plane, if $\mathrm{Im}\{\kappa_j\}>0$ and $\mathrm{Re}\{\kappa_j\}>0$. Using the relations between the eigenvectors in Table 1, the combined input power, $P_a+P_b$, from the poles, $\kappa_j$ and $-\kappa_j^*$, is thus given by

$$P_a+P_b=\frac{\omega}{2}\mathrm{Re}\left(\frac{\boldsymbol{\theta}_j^{\mathrm{T}}\mathbf{f}_0\mathbf{f}_0^{\mathrm{H}}\boldsymbol{\varphi}_j}{\boldsymbol{\theta}_j^{\mathrm{T}}\mathbf{D}'(\kappa_j)\boldsymbol{\varphi}_j}\right)+\frac{\omega}{2}\mathrm{Re}\left(\frac{\boldsymbol{\theta}_j^{\mathrm{H}}\mathbf{f}_0\mathbf{f}_0^{\mathrm{H}}\boldsymbol{\varphi}_j^*}{\boldsymbol{\theta}_j^{\mathrm{H}}\mathbf{D}'(-\kappa_j^*)\boldsymbol{\varphi}_j^*}\right).$$

Furthermore,

$$\mathrm{Re}\left(\frac{\boldsymbol{\theta}_j^{\mathrm{H}}\mathbf{f}_0\mathbf{f}_0^{\mathrm{H}}\boldsymbol{\varphi}_j^*}{\boldsymbol{\theta}_j^{\mathrm{H}}\mathbf{D}'(-\kappa_j^*)\boldsymbol{\varphi}_j^*}\right)=\mathrm{Re}\left(\frac{(\boldsymbol{\theta}_j^{\mathrm{H}}\mathbf{f}_0\mathbf{f}_0^{\mathrm{H}}\boldsymbol{\varphi}_j^*)^*}{(\boldsymbol{\theta}_j^{\mathrm{H}}\mathbf{D}'(-\kappa_j^*)\boldsymbol{\varphi}_j^*)^*}\right)=\mathrm{Re}\left(\frac{\boldsymbol{\theta}_j^{\mathrm{T}}\mathbf{f}_0\mathbf{f}_0^{\mathrm{H}}\boldsymbol{\varphi}_j}{\boldsymbol{\theta}_j^{\mathrm{T}}(\mathbf{D}'(-\kappa_j^*))^*\boldsymbol{\varphi}_j}\right)$$

and

$$(\mathbf{D}(-\kappa_j^*))^*=-\mathbf{D}'(\kappa_j),$$

which is verified by direct substitution in Eq. (34) for $\eta=0$.

It follows that

$$P_a+P_b=P_a-P_a=0.$$

## References


[1] L. Cremer, M. Heckl, E.E. Ungar, *Structure-Borne Sound*, Springer, Berlin, 1988.
[2] R.H. Lyon, R.G. DeJong, *Theory and Application of SEA*, Butterworth-Heinemann, London, 1995.
[3] R.J.M. Craik, *Sound Transmission through Buildings Using Statistical Energy Analysis*, Gower, London, 1996.
[4] F.J. Fahy, Statistical energy analysis: a wolf in sheep's clothing? *Proceedings of the InterNoise*, Leuven, 1993.
[5] B.R. Mace, P. J Shorter, Energy flow models from finite element analysis, *Journal of Sound and Vibration* 233 (2000) 369–389.
[6] S. Finnveden, Statistical energy analysis of fluid-filled pipes, in: F.J. Fahy, W.G. Price (Eds.), *IUTAM Symposium on Statistical Energy Analysis*, Kluwer Academic Publishers, Dordrecht, 1999, pp. 289–300.
[7] R.S. Langley, On the power input to point loaded hysteretically damped structures, *Journal of Sound and Vibration* 181 (1995) 657–672.
[8] B. Aalami, Waves in prismatic guides of arbitrary cross section, *Journal of Applied Mechanics* 40 (1973) 1067–1072.
[9] S.K. Datta, A.H. Shah, R.L. Bratton, T. Chakraborty, Wave propagation in laminated composite plates, *Journal of the Acoustical Society of America* 83 (1988) 2020–2026.
[10] L. Gavric, Finite element computation of dispersion properties of thin-walled waveguides, *Journal of Sound and Vibration* 173 (1994) 113–124.
[11] L. Gavric, Computation of propagative waves in free rail using a finite element technique, *Journal of Sound and Vibration* 184 (1995) 531–543.
[12] U. Orrenius, S. Finnveden, Calculation of wave propagation in rib-stiffened plate structures, *Journal of Sound and Vibration* 198 (1996) 203–224.
[13] O. Onipede, S.B. Dong, Propagating waves and end modes in pretwisted beams, *Journal of Sound and Vibration* 195 (1996) 313–330.
[14] T. Mazuch, Wave dispersion in anisotropic shells and rods by the finite element method, *Journal of Sound and Vibration* 198 (1996) 429–438.
[15] V.V. Volovoi, D.H. Hodges, V.L. Berdichevsky, V.G. Sutyrin, Dynamic dispersion curves for non-homogenous, anisotropic beams with cross-section of arbitrary geometry, *Journal of Sound and Vibration* 215 (1998) 1101–1120.
[16] C.-M. Nilsson, Waveguide Finite Elements for Thin-walled Structures, Licentiate Thesis, MWL, KTH, 2002.
[17] C.-M. Nilsson, S. Finnveden, Tyre vibration modelling with conical waveguide finite elements, *Proceedings of the InterNoise, Detroit*, *Paper N179*, 2002.
[18] C.-M. Nilsson, S. Finnveden, Waveguide finite elements for fluid and fluid–shell coupling, *Proceedings of the ICSV10, Stockholm*, 2003.
[19] S. Finnveden, Evaluation of modal density and group velocity by a finite element method, *Journal of Sound and Vibration* 273 (2004) 51–75.
[20] P.M. Morse, H. Feshbach, *Methods of Theoretical Physics*, McGraw-Hill, New York, 1953.
[21] G.M.L. Gladwell, A variational formulation for damped acusto-structural problems, *Journal of Sound and Vibration* 4 (1966) 172–186.
[22] S. Finnveden, Exact spectral finite element analysis of stationary vibrations in a railway car structure, *Acta Acustica* 2 (1994) 461–482.
[23] R.D. Cook, D.S. Malkus, M.E. Plescha, *Concepts and Applications of Finite Element Analysis*, third ed., Wiley, New York, 1989.
[24] I. Karasalo, Exact finite elements for wave propagation in range-independent fluid–solid media, *Journal of Sound and Vibration* 172 (1994) 671–688.
[25] F.R. Gantmacher, *Applications of the Theory of Matrices*, Interscience, New York, 1959.
[26] R.S. Langley, Wave motion and energy flow in cylindrical shells, *Journal of Sound and Vibration* 169 (1994) 29–42.